Correlating Structure with Photovoltaic Properties in Phase-Separated Blends of Conjugated Donor Polymer and Acceptor

Jihun Jeon,[1] Kiyotaka Doi,[1] Hyung Do Kim,[1] Hiroki Ogawa,[2] Mikihito Takenaka,[2] Hideo Ohkita[1]

[1] Graduate School of Engineering, Department of Polymer Chemistry, Kyoto University, Katsura, Nishikyo-ku, Kyoto 615-8510, Japan.

[2] Institute for Chemical Research, Kyoto University, Gokasho, Uji, Kyoto 611-0011, Japan.

Contact

Hyung Do Kim: hyungdokim@photo.polym.kyoto-u.ac.jp

Hideo Ohkita: ohkita@photo.polym.kyoto-u.ac.jp

Abstract

A power conversion efficiency of polymer solar cells strongly depends on the microscale morphology of interpenetrating network structures between polymer donor and acceptor materials. It is therefore essential to understand the relationship between photovoltaic properties and phase-separated structures in the blend active layer. Here, we discuss the relationship between charge generation and collection and phase-separated structures analyzed by a ternary phase diagram for polymer solar cells based on blends of a thiophene-based conjugated polymer donor P3HT or PDCBT and three different acceptors: a fullerene derivative PCBM, a nonfullerene acceptor ITIC, and a conjugated polymer acceptor N2200. By considering the ternary phase diagram based on the Flory–Huggins interaction parameters, we discuss binodal point and acceptor volume fraction in mixed-phase in each material combination. Furthermore, we suggest strategies for improving the efficiency of polymer solar cells according to the molecular weight of acceptor materials. These findings will be a guideline for highly efficient polymer solar cells.

Key Words: Polymer solar cell, Charge generation, Charge collection, Phase-separated structure, Ternary phase diagram

Introduction

Recently, polymer solar cells based on blends of a conjugated donor polymer and an acceptor material have been regarded as one of the most brilliant next-generation energy sources since they have plenty of advantages, inclusive of high flexibility, lightweight, and cost-effective manufacturing process.[1–4] Initially, intensive research efforts have been devoted to developing highly efficient polymer solar cells based on fullerene derivatives. Consequently, their power conversion efficiency (PCE) has been remarkably improved over the past decade, and exceeded 12% at the beginning of 2010 even for single-junction cells.[5] For such fullerene-based polymer solar cells, however, further improvements in PCE have been limited because fullerene derivatives have low light-harvesting efficiency in the visible and near-infrared (near-IR) regions and limited control of energy level.[6,7] To overcome such limitations, various conjugated acceptor polymers and nonfullerene acceptors (NFAs), which can harvest many more photons from the visible to near-IR region of the solar spectrum, have been designed and synthesized as alternatives to fullerene derivatives. As a result, the devices based on these materials exhibit high light-harvesting efficiency in the visible and near-IR regions, thereby yielding a substantial increase in PCE up to ~16% for devices based on conjugated acceptor polymers and ~19% for devices based on NFAs.[8,9]

For further improvements in PCE, short-circuit current density (J_{SC}), open-circuit voltage (V_{OC}), and fill factor (FF) should be improved simultaneously. Among them, J_{SC} and FF are in trade-off relationship: thicker active layers would improve J_{SC} but degrade FF. In other words, there is a trade-off relationship between charge generation and collection efficiencies (η_{CG} and η_{CC}). In terms of blend morphology, a large phase-separated domain is beneficial for η_{CC} while it is rather undesirable for η_{CG} because charge carriers are likely to be transported efficiently to each electrode but most of excitons generated cannot arrive at a donor/acceptor interface in such a large domain. Thus, of particular importance is to optimize domain size in blend films. Such phase-separated domain size would be dependent upon inherent characteristics of materials employed. In the case of polymer/polymer blends, for example, the enthalpy term is likely to be positive to promote phase separation while the entropy term is negative to promote mixing but negligibly small according to the Flory–Huggins theory, giving rise to phase separation on a micrometer scale, which has a negative impact on η_{CG}.[10] As such, the phase-separated structure is very closely related to photovoltaic performance for polymer solar cells. For achieving highly efficient polymer solar cells, it is, therefore, of paramount importance to understand the correlation between phase-separated structures and photovoltaic conversion processes from a viewpoint of thermodynamics of phase separation during film-forming.

Herein, we focus on three types of polymer solar cells based on blends of polymer/fullerene, polymer/NFA, and polymer/polymer to discuss the relationship between photovoltaic parameters and blend

morphology.   More specifically, we fabricated polymer solar cells by using thiophene-based conjugated polymer donors (P3HT or PDCBT), a fullerene derivative (PCBM), an NFA (ITIC), and a naphthalene diimide-based conjugated polymer acceptor (N2200), as shown in **Figure 1a**, and then measured photovoltaic performance under AM1.5G simulated solar illumination at 100 mW cm^{-2}.   As a result, we found that PDCBT-based solar cells exhibit PCE higher than P3HT-based solar cells without regard to electron acceptor materials employed.   In addition, the photovoltaic performance is significantly dependent on acceptor materials used; it is higher in the devices based on PCBM and/or ITIC than in those based on N2200.   In particular, there is a large difference in PCE between PDCBT/ITIC and P3HT/ITIC solar cells.   To disclose the origin of such different photovoltaic properties in more detail, we first estimated η_{CG} and η_{CC} by evaluating photoluminescence (PL) quenching efficiency (Φ_q) and the ratio of J_{SC} to the reverse saturation photocurrent density ($J_{ph,sat}$), respectively.   Subsequently, we measured differential scanning calorimetry (DSC) to obtain ternary phase diagrams for solvent/donor/acceptor by using Flory–Huggins interaction parameters (χ) between the components that govern phase behavior for the blend system.   As a result, we found that η_{CG} is correlated with the binodal point and that η_{CC} is closely related to the volume fraction of the acceptor in the mixed-phase.   On the basis of our findings, we further suggest potential strategies for improving the photovoltaic performance of polymer solar cells in terms of phase separation.

Materials and methods

Materials and device preparation

The donor materials employed were poly(3-hexylthiophene-2,5-diyl) (P3HT, M_w = 44,000, M_n = 22,000, PDI = 2.0) and poly[2,2′′′′-bis[[(2-butyloctyl)oxy]carbonyl]-[2,2′:5′,2′′:5′′,2′′′-quaterthiophene]-5,5′′′-diyl] (PDCBT, M_w = 60,000, M_n = 24,000, PDI = 2.5) purchased from Sigma Aldrich and 1-Materials, respectively.   The acceptor materials employed were [6,6]-phenyl-C$_{61}$-butyric acid methyl ester (PCBM) purchased from Frontier Carbon, 2,2′-[[6,6,12,12-tetrakis(4-hexylphenyl)-6,12-dihydrodithieno[2,3-d:2′,3′-d']-s-indaceno[1,2-b:5,6-b']dithiophene-2,8-diyl]bis[methylidyne(3-oxo-1H-indene-2,1(3H)-diylidene)]]bis[propanedinitrile] (ITIC) purchased from Solarmer Energy, Inc, and poly{[N,N'-bis(2-octyldodecyl)-naphthalene-1,4,5,8-bis(dicarboximide)-2,6-diyl]-alt-5,5′-(2,2′-bithiophene)} (N2200, M_w = 125,000, M_n = 54,400, PDI = 2.3) purchased from Ossila.   The interlayer materials employed were poly(3,4-ethylenedioxythiophene):poly(4-styrenesulfonate) (PEDOT:PSS, PH-500) purchased from H.C. Stark,   and   Poly[(9,9-bis(3'-((N,N-dimethyl)-N-ethylammonium)-propyl)-2,7-fluorene)-alt-2,7-(9,9-dioctylfluorene)]   (PFN-Br)   purchased   from   Solarmer   Energy,   Inc.   Chlorobenzene (CB), o-dichlorobenzene (DCB), toluene, acetone, and ethanol were purchased from Nacalai Tesque.

The solar cells with the layered structure of ITO/PEDOT:PSS/active layer/PFN-Br/Al were prepared for photovoltaic performance measurements.   Indium–tin-oxide (ITO)-coated glass substrates were washed by ultrasonication in toluene, acetone, and ethanol for 15 min each in this order, and then dried with N$_2$ flow.   The washed ITO substrates were treated with a UV–O$_3$ cleaner (Nippon Laser & Electronics Lab., NL-UV253S) for 30 min.   A thin layer (~30 nm) of PEDOT:PSS was spin-coated onto the ITO glass substrates at a spin rate of 3000 rpm for 99 s, and then annealed at 150 °C for 10 min in air.   Subsequently, PEDOT:PSS coated ITO glass substrates were moved to a nitrogen-purged glovebox.   A donor/acceptor blend layer was spin-coated from a DCB solution on the top of the PEDOT:PSS layer.   The blend solution was prepared by dissolving the donor and acceptor materials in DCB with a volume ratio of 1 to 1.   Sequentially, the interlayer was spin-coated on top of the active layer without any further treatments.   The interlayer solution was prepared by dissolving PFN-Br in anhydrous methanol with a concentration of 0.5 mg mL^{-1}.   Finally, 100 nm of Al cathode was thermally deposited on the top of the interlayer at a pressure of ~4 × 10^{-4} Pa with a shadow mask to ensure the electrode area 0.07 cm^2.   The current density–voltage (J–V) characteristics of the devices were measured with a DC voltage and current source/meter (Keithley, 2611B) in the dark and under AM 1.5G simulated solar illumination at 100 mW cm^{-2} (Bunko-Keiki, ECT-25WB).   The light intensity was corrected with a calibrated silicon photodiode reference cell (Bunko-

Keiki, BS-520).

The melting temperature of samples was evaluated with a DSC instrument (PerkinElmer, DSC8500-S). For solid/liquid samples (donor or acceptor and DCB), 5 mg of the solid material were loaded into an Al sample pan together with 0.5, 1, 3, and 7 mL of DCB. To prevent solvent evaporation during the measurement, the sample was sealed under high pressure. For the solid/solid samples (donor and acceptor), on the other hand, donor/acceptor blend films were prepared by drop cast from blend solutions with different volume ratios and dried for 48 h to ensure solvent evaporation. All films were scratched off, loaded into an Al sample pan, and sealed under high pressure. All samples were heated from 50 °C to a temperature above each melting temperature together with an empty Al pan as a reference. The measurements were carried out at a heating rate of 10 K min^{-1} in a nitrogen flow of 20 mL min^{-1}. The melting point of each sample was evaluated from the intersection point between the baseline and tangent at the inflection point of the DSC curve.[11]

Results and discussion

Absorption Spectra and Energy Diagrams

Figure 1b shows absorption spectra of two donor and three acceptor materials employed in this study. The donor polymers P3HT and PDCBT exhibit similar absorption bands in the visible range from 350 to 650 nm with a vibronic shoulder at around 600 nm, which are indicative of a high crystallinity. On the other hand, PCBM exhibits an absoption band in the UV region but a small absorption tail in the visible region while ITIC and N2200 exhibit an absorption band at around 700 nm. This absorption band is well complemented with the donor absorption, leading to extended light-harvesting region. In particular, no noticeable vibronic stuctures were observed for ITIC and N2200, indicating a moderate or less aggregation. The highest occupied molecular orbital (HOMO) and lowest unoccupied molecular orbital (LUMO) energy level (E_{HOMO} and E_{LUMO}) of each material are summarized in **Figure 1c**. The E_{HOMO} of the donor and acceptor materials was evaluated by photoelectron yield spectroscopy, and the E_{LUMO} of the donor materials was estimated from the E_{HOMO} and an optical bandgap energy (E_g^{opt}) based on the 0–0 transition absorption peaks, and the E_{LUMO} of the acceptor materials was evaluated by cyclic voltammetry. As shown in **Figure 1c** (see also **Figure S1**), the E_{HOMO} was deeper for PDCBT (−5.15 eV) than that for P3HT (−4.69 eV) because of an introduction of electron-withdrawing carboxylate substituents to the side chain.[12] In contrast, no large difference in the E_{LUMO} was observed for the acceptor materials, which was evaluated to be ranging from −3.78 to −3.96 eV. In particular, there is a sufficient energetic offset in E_{LUMO} between donor and acceptor materials that are enough to cause efficient charge transfer at the heterojunction of donor and acceptor materials.

Photovoltaic Performance

Figure 2 and **S2** shows *J–V* chacteristics and incident photon-to-current conversion efficiency (IPCE) spectra of a series of polymer solar cells based on crystalline donor polymers with different side chains and three different acceptor materials. As summarized in **Table 1**, photovoltaic performance of PDCBT-based solar cells overwhelmed that of P3HT-based solar cells without regard to acceptor materials employed, mainly because of larger J_{SC} and V_{OC}. The improved V_{OC} in PDCBT blends is simply because of the deeper HOMO level of the PDCBT polymer. The improvement in J_{SC} is mainly ascribable to the enhanced η_{CG}, as will be decribed later in more detail. Notably, the photovoltaic performance is considerably dependent upon acceptor materials employed. More specifically, PCBM-based solar cells exhibited the highest photovoltaic performance due to the highest FF as well as a moderate J_{SC} while N2200-based solar cells exhibited the lowest PCE less than 1% as a result of the lowest J_{SC} and FF. On ther other hand, ITIC-based solar cells provided an intermediate photovoltaic performance among them. Interestingly, a definite

difference in J_{SC} was found between P3HT/ITIC and PDCBT/ITIC solar cells, which will be discussed later in more detail.

Charge generation and collection efficiency

To address the origin of the difference in J_{SC} for these solar cells, we evaluated PL quenching efficiency Φ_q of each blend film. The samples were excited at 500, 340, 700 and 700 nm for selective excitation of donor polymers, PCBM, ITIC, and N2200, respectively. Detailed PL spectra of each neat and blend film can be found in **Figure S3**. Note that the Φ_q is a good measure for η_{CG}, which is a product of exciton diffusion efficiency (η_{ED}) and charge transfer efficiency (η_{CT}). In most cases, η_{CT} can be assumed to be 100% if there is enough energy offset in HOMO or LUMO levels between donor and acceptor materials. As this is true for all the blends, the Φ_q can be ascribed to η_{ED} in this study. As shown in **Table 2**, Φ_q^D of the selective excitation of donor polymers was estimated to be more than ~90% except for the P3HT/N2200 blend. This is ascribed to long-range energy transfer from donor polymers to acceptors because of the large spectral overlap between the donor emission and acceptor absorption bands. Considering contribution of the energy transfer to Φ_q^D and Φ_q^A, we assumed that η_{CG} (η_{ED}) can be estimated to be a product of Φ_q^D and Φ_q^A except for PCBM-based blends and can be estimated as Φ_q^D for PCBM-based blends because of no energy transfer from PCBM to donor polymer. We therefore conclude that the higher J_{SC} in PDCBT-based blends is partly due to the relatively larger η_{ED} than that of P3HT-based blends, because the PDCBT-based blends would be likely to form phase-separated domains smaller than the P3HT-based blends.

As shown in **Figure 3**, the absorption band of ITIC in the P3HT/ITIC blend film is much blue-shifted compare to that of the ITIC neat film, suggesting that ITIC molecules are likely not to be aggregated but rather molecularly dispersed in the P3HT/ITIC blend film. This finding suggests that the Φ_q^A for P3HT/ITIC is not reliable because the PL quantum yield may be different between ITIC neat and P3HT/ITIC blend films. We therefore do not adopt the Φ_q^A for P3HT/ITIC for the following discussion.

To evaluate η_{CC} in all the polymer blends studied, we measured J–V characteristics over a wide voltage region under the simulated solar illumination. The $J_{ph,sat}$ was estimated by using the Hecht equation[13] where J_{ph} is the difference between the photocurrent density and the dark current density, V_{in} is assumed to be $V - V_{OC}$, $\mu\tau V_{in}/d$ is the mean free path of charge carriers, and d is the active layer thickness (the average transit distance is $d/2$).

$$J_{ph} = J_{ph,sat} \frac{\mu\tau V_{in}}{d} \Big/ \frac{d}{2} \left[1 - \exp\left(-\frac{d}{2} \Big/ \frac{d}{\mu\tau V_{in}} \right) \right] \tag{1}$$

Figure 4 shows the J_{ph}–V_{in} curve with the fitting curve based on Eq. 1 for various polymer solar cells. As summarized in **Table 2**, the η_{CC} of PDCBT blends is greater than that of P3HT blends, regardless of acceptor materials employed. As for acceptor materials, the η_{CC} was highest for PCBM-based blends, and about the same between ITIC- and N2200-based blends. This would be partly due to higher electron mobility of PCBM.[14] However, the lower η_{CC} in N2200-based blends is not consistent with high electron mobility of N2200.[15] Thus, this should be rather related to blend morphology rather than materials properties as will be discussed later.

Furthermore, we can see a certain tendency that the J_{SC} is correlated to the product of η_{ED} and η_{CC}. Comparing PDCBT- and P3HT-based solar cells, for example, the larger J_{SC} is consistent with the larger product of η_{ED} and η_{CC}. In addition, we can see another tendency that the FF is correlated to the η_{CC}. For example, PCBM-based solar cells exhibit the highest FF, which is consistent with the largest η_{CC}. This tendency suggests that the η_{CC} can be well reproduced by the Hecht equation. On the other hand, there are some discrepancies in these tendencies as well: in contrast to the product of η_{ED} and η_{CC}, i) J_{SC} of P3HT/ITIC is too low, ii) the experimental J_{SC} of P3HT/ITIC is higher than that of PDCBT/PCBM. The low J_{SC} of P3HT/ITIC is probably due to low charge dissociation efficiency in P3HT/ITIC where ITIC are

not aggregated but rather molecularly dispersed as mentioned above.   The high J_{SC} of P3HT/ITIC is partly because of different absorption ranges between them.   In this study, we focus on the overall tendencies rather than individual minor discrepancies.

Thermodynamic miscibility between donor, acceptor, and solvent

As described before, the η_{ED} and η_{CC} are closely related to phase-separated structures in polymer blends. We therefore consider thermodynamic miscibility between donor, acceptor, and solvent to discuss phase-separated structures in various polymer blends studied.   The thermodynamic miscibility was analyzed on the basis of the Flory–Huggins interaction parameter χ.   The larger χ_{12} indicates lower miscibility between components 1 and 2, which can be an advantage in terms of domain purity.   In this study, we evaluate the χ parameters by using the melting point depression equation.[16]   In general, the melting point of crystalline materials is depressed by the reduction of chemical potential when blended with minor materials.   Thus, the χ parameter can be evaluated from the melting point change due to the volume fraction change.   The melting point reduction was measured by DSC measurements for the various binary blends of donor, acceptor, and solvent.

Figure 5 shows DSC heat flow of PDCBT measured over a wide temperature range.   As shown in the figure, we evaluated the melting point from the intersection point between the baseline and tangent at the inflection point of the DSC curve.   The χ parameter can be estimated by Eq 2 with the melting points and volume fractions[16]

$$\frac{1}{T_m} - \frac{1}{T_m{}^0} = -\frac{RV_{2u}}{\Delta H_{2f} V_{1u}} \times \left[\frac{\ln \varphi_2}{m_2} + \left(\frac{1}{m_2} - \frac{1}{m_1} \right)(1 - \varphi_2) + \chi_{12}(1 - \varphi_2)^2 \right] \tag{2}$$

where T_m is melting point when mixed with a minor material, $T_m{}^0$ is melting point of the pure material, V_u is the molar volume of repeating unit for polymer, ΔH_f is the enthalpy of fusion per mole for pure crystalline, φ is volume fraction, m_i is the degree of polymerization of component i, and R is gas constant.

As summarized in **Table 3** and **Figure S4**, the χ parameter between the solvent and donor polymers is relatively low, indicating that DCB is a good solvent for the donor polymers employed.   However, the χ parameter between the solvent and acceptors is quite high, especially for N2200, implying that N2200 is likely to form aggregates even in DCB solutions.   Among them, PCBM and ITIC exhibit relatively good miscibility with DCB.   This is probably due to polar groups in PCBM and ITIC molecules.   In terms of thermodynamic miscibility between donor and acceptor materials, N2200 is most well-miscible with donor polymers regardless of them, meanwhile, PCBM is most immiscible.

Ternary phase diagram and phase separation

The Flory–Huggins mean-field theory[17] postulates that the enthalpy contribution to the free energy of mixing (ΔG_m) of a system composed of different two types of substances dissolved in a particular solvent depends on the interactions between the components given by the interaction parameter χ_{12}.   The ΔG_m is given by,[17]

$$\frac{\Delta G_m}{k_B T} = \frac{1}{N_1}\varphi_1 \ln\varphi_1 + \frac{1}{N_2}\varphi_2 \ln\varphi_2 + \varphi_3 \ln\varphi_3 + \varphi_1\varphi_2\chi_{12} + \varphi_1\varphi_3\chi_{13} + \varphi_2\varphi_3\chi_{23} \tag{3}$$

where k_B is the Boltzmann constant, T is absolute temperature, N_1 and N_2 are the effective molecular size of the components 1 and 2 in the lattice sites, and φ_i is the volume fraction of the component i (i = 1 and 2: polymers, i =3: solvent).   The coexistence curve (binodal line) can be obtained under the equilibrium condition of chemical potential between two phases.[17–21]   On the basis of the χ parameters evaluated by the melting point depression equation, we obtained ternary phase diagrams to discuss the phase separation behavior of the P3HT and PDCBT blends in different three acceptor materials.

Figure 6 shows the ternary phase diagrams for three components of solvent/donor/acceptor systems. The solid line represents the binodal line of the one-phase stable region and two-phase stable region for the different acceptor blends.　A vertical line corresponds to a drying pathway of polymer solution during the spin-coating with a volume fraction of polymer to acceptor materials (v/v 1 : 1).　During the spin-coating, phase-separation starts at the intersection point of the drying pathway and binodal line, since the outer of the binodal line is a one-phase stable region and the inner of that is a two-phase stable region.　At the beginning of the spin-coating, the ternary solvent/donor/acceptor mixture is homogeneous because the solvent is present in the majority.　At the intersection point between the drying pathway and binodal line in the ternary phase diagram, the mixture undergoes internal phase separation into mixed-phase and pure acceptor-phase.[22–25]　Note that the thickness of active layers was adjusted to be about 50 – 70 nm for all the polymer blends as summarized in **Table S2** in order to minimize the effect of thickness on the phase separation.　In addition, phase-separated structures were clearly observed as shown in **Figure S5**, suggesting surface segregation is not dominant in these blend films.　We thus can safely discuss the phase separation in terms of intermolecular interaction.　We also note that the self-diffusion coefficient of each component in the solvent is almost the same, and the diffusion on phase separation is governed by the thermodynamic driving force.　Thus, the domain size would be larger as the phase-separation time is longer,[26] and hence the domain size of each polymer blend can be predicted from the intersection point. As shown in figure, the intersection point is found earlier in the order of solvent/donor/N2200, solvent/donor/ITIC, and solvent/donor/PCBM, except for the dispersed DCB/P3HT/ITIC system. Comparing P3HT with PDCBT systems, the intersection point is found earlier in the solvent/P3HT/acceptor. These results are consistent with the η_{ED} observed for each blend described before.　Specifically, for example, excitons in N2200 blends would be deactivated before reaching a donor/acceptor interface because of a large phase-separated domain and a shorter diffusion length of N2200 excitons.[27]

We next focus on the closed circles in the ternary phase diagrams in **Figure 6**, which represent an acceptor volume fraction ($\varphi_{acceptor}$) in mixed-phase after the phase-separation is completed.　**Figure 7** illustrates a phase-separated structure in mixed-phase according to the acceptor volume fraction.　For the N2200 blends, $\varphi_{acceptor}$ in mixed-phase was almost zero, regardless of the donor polymer.　As shown in **Figure 7a**, electron carriers cannot be transported in the mixed-phase and hence η_{CC} would be degraded because of isolated and discontinuous acceptor materials.[28]　For the ITIC blends, on the other hand, $\varphi_{acceptor}$ in the mixed-phase was more than 0.3 regardless of the donor polymer.　As shown in **Figure 7b**, acceptor molecules would be well-connected but at the same time donor molecules would be disconnected, resulting in severe bimolecular recombination and hence less η_{CC}.[29]　For the PCBM blends, $\varphi_{acceptor}$ in the mixed-phase was ranging from 0.1 to 0.2 regardless of the donor polymer, which corresponds to the percolation threshold, as reported previously.[30]　As shown in **Figure 7c**, it can be expected that the charge transport occurs effectively with suppressed bimolecular recombination in the range of percolation threshold. Furthermore, it can be seen that P3HT/ITIC blend has exceptionally large $\varphi_{acceptor}$ in the mixed-phase, which supported the dispersed phase-separation in P3HT/ITIC blend.　These $\varphi_{acceptor}$ in the mixed-phase are in good agreement with the η_{CC} observed.　Consequently, we conclude that the $\varphi_{acceptor}$ is a good measure for the miscibility between the donor polymer and acceptor.

Charge generation efficiency, charge collection efficiency and phase-separated structure

We next consider the solubility parameter to discuss the improvement in η_{ED} according to the acceptor molecular weight.　Here, we focus on PCBM as a small molecule acceptor and N2200 as a polymer acceptor.　The χ_{12} is related to the difference in the solubility parameters $\Delta\delta_{12}$, which is given by equation (4),[31]

$$\chi_{12} \propto \Delta\delta_{12} = \sqrt{(\delta_{D1} - \delta_{D2})^2 + (\delta_{P1} - \delta_{P2})^2 + (\delta_{H1} - \delta_{H2})^2} \tag{4}$$

where δ_{Di}, δ_{Pi}, and δ_{Hi} ($i = 1$ and 2) represent the dispersion contribution, polar contribution, and hydrogen bonding contribution of the components i.　**Table S3** shows the solubility parameters of the two acceptor

materials used in this study, PCBM and N2200, and two solvents DCB and CB for comparison.[32,33]   As summarized in the table, the dispersion contribution δ_D is the largest in the all the materials, the hydrogen-bonding contribution δ_H is the second largest in the acceptor materials, and the polar contribution δ_P is the second largest in the solvents.   As summarized in **Table S3**, the $\Delta\delta_{acceptor-solvent}$ is smaller when CB is employed as a solvent because of the smaller difference in δ_P of solubility parameter between solvent and acceptor materials, regardless of the types of acceptors.   This result implies that the lower $\chi_{acceptor-solvent}$ when CB is employed as a solvent.   **Figures S6** shows the ternary phase diagram of the solvent/P3HT/PCBM and solvent/P3HT/N2200 system with the binodal point based on the different $\chi_{acceptor-solvent}$.   We note that the binodal point represents the phase separation starting point.   As shown in the figures, the binodal point is downshifted in the drying pathway if CB was used instead to DCB, which would result in a smaller domain size regardless of acceptor employed.   In other words, the smaller $\chi_{acceptor-solvent}$ can delay the phase reparation, resulting in a smaller domain size and therefore, the exciton diffusion property would be better.   Consequently, it is expected to improve the η_{ED}, and hence η_{CG}, by using solvent that have smaller difference in solubility parameter.

Furthermore, as mentioned above, it is appropriate that the $\varphi_{acceptor}$ in the mixed-phase is ranging between 0.1 and 0.2 for efficient charge collection.[30]   From the ternary phase diagram, it can be seen that $\varphi_{acceptor}$ in the mixed-phase was estimated to be 0.1–0.2 in PCBM blends, more than 0.3 in ITIC blends, and almost 0 in N2200 blends, regardless of donor polymers.   **Figures 8a and S7** show the binodal line plotted against the volume fraction of the small molecular weight acceptor. In order to achieve the $\varphi_{acceptor}$ of 0.1–0.2 in the mixed-phase, we need materials combination with a $\chi_{donor-acceptor}$ of 1.4–1.9 for P3HT/PCBM and of 1.37–1.85 for P3HT/ITIC blends.   At room temperature, $\chi_{donor-acceptor}$ is estimated to be 1.68 for P3HT/PCBM, and to be 0.84 for P3HT/ITIC blends.   Consequently, appropriate percolation pathways are likely to be formed in the mixed phase in the P3HT/PCBM blend, resulting in effective charge collection. On the other hand, P3HT and ITIC are likely to be too mixed in the mixed phase in the P3HT/ITIC blend, resulting in increasing bimolecular recombination.   This is consistent with the blue-shifted absorption band observed for the P3HT/ITIC blend film.   On the other hand, as shown in **Figure 8b**, even if the value of $\chi_{donor-acceptor}$ is quite small to 0.1 or less, the phase is separated into the pure phase in the P3HT/N2200 blends.   In fact, $\chi_{donor-acceptor}$ of P3HT/N2200 is estimated to be 0.17 at room temperature, which represents much more severe phase separation in P3HT/N2200 blends.   These severe phase separation structures are disadvantageous in terms of η_{CC}, because the acceptor domain in the mixed-phase cannot connect continuously, and hence electron transfer is hindered.[28]   For this, it is necessary to frozen the phase separation in a non-equilibrium state.   This could be achieved by cooling the material down to the glass transition temperature (T_g).   At temperatures lower than T_g, the change in volume fraction due to phase separation is stopped because the main chain motion of the polymer is frozen.   Therefore, a polymer with a high T_g would be beneficial for η_{CC}.   We therefore suggest that the $\chi_{acceptor-solvent}$ should be reduced and use a polymer acceptor with a high T_g, in order to achieve a high PCE value.

Conclusion

In summary, we discussed the relationship between the charge generation and collection properties and the thermodynamic miscibility for various polymer blends on the basis of ternary phase diagrams.   The J–V characteristics was evaluated as higher PCE for the PDCBT blend with the advantage of J_{SC}, regardless of acceptor material.   The overall J_{SC} tendency is consistent with the η_{CG} and η_{CC} product.   Focusing on such overall tendency, we evaluated the thermodynamic miscibility through the ternary phase diagram by using the χ parameter, since the η_{ED} and η_{CC} are closely related to thermodynamic miscibility.   From the binodal point in the ternary phase diagram, it can be said that later phase separation results in smaller domain size, leading to higher η_{ED}.   In PCBM blends, the $\varphi_{acceptor}$ in the mixed-phase was 0.1–0.2, which corresponds to a percolation threshold at which charge collection would be efficient.   In ITIC blends, on the other hand, it was more than 0.3, suggesting that bimolecular recombination would be dominant in competition with the charge collection.   In N2200 blends, it was close to zero, suggesting that acceptor molecules are likely to be isolated in the mixed-phase and hence electrons are difficult to be transported to

electrode.   On the basis of these findings, we propose strategies for improving PCE in polymer solar cells via improvement in η_{ED} and η_{CC}.   For small molecule acceptors, a good solvent would be beneficial for delayed phase separation to obtain moderately small domains and thus achieve high η_{ED}.   For polymer acceptors, such delayed phase separation would be beneficial as is the case of small molecule acceptors but actually should be difficult to be achieved because of the large number of repeating units.   Instead, we therefore suggest polymer acceptors with higher T_g would be beneficial for such delayed phase separation to increase η_{CC}.

Acknowledgments

Reference

1. Sondergaard, R., Hosel, M., Angmo, D., Larsen-Olsen, T. T., Krebs, F. C.   Roll-to-roll fabrication of polymer solar cells. Mater Today 2012;15:36–49.

2. Kaltenbrunner, M., White, M. S., Głowacki, E. D., Sekitani, T., Someya, T., Sariciftci, N. S., Bauer, S. Ultrathin and lightweight organic solar cells with high flexibility. Nat Commun 2012;3:770.

3. Kang, H., Kim, G., Kim, J., Kwon, S., Kim, H., Lee, K. Bulk-Heterojunction Organic Solar Cells: Five Core Technologies for Their Commercialization. Adv Mater 2016;28:7821–7861.

4. Kim, T., Kim, J.-H., Kang, T.   E., Lee, C., Kang, H., Shin, M., Wang, C., Ma, B., Jeong, U., Kim, T.-S. Kim, B. J. Flexible, Highly Efficient All-Polymer Solar Cells. Nat Commun 2015;6:8547.

5. Zhao, J., Li, Y., Yang, G., Jiang, K., Lin, H., Ade, H., Ma, W., Yan, H. Efficient Organic Solar Cells Processed from Hydrocarbon Solvents. Nat Energy 2016;1:15027.

6. He, Y., Chen, H.-Y., Hou, J., Li, Y. Indene−C60 Bisadduct: A New Acceptor for High-Performance Polymer Solar Cells. J Am Chem Soc 2010;132:5532–5532.

7. He, Y., Li, Y. Fullerene Derivative Acceptors for High Performance Polymer Solar Cells. Phys Chem Chem Phys 2011;13:1970–1983.

8. Cui, Y., Xu, Y., Yao, H., Bi, P., Hong, L., Zhang, J., Zu, Y., Zhang, T., Qin, J., Ren, J., Chen, Z., He, C., Hao, X., Wei, Z., Hou, J. Single-Junction Organic Photovoltaic Cell with 19% Efficiency. Adv Mater 2021;33:2102420.

9. Jia, T., Zhang, J., Zhang, K., Tang, H., Dong, S., Tan, C.-H., Wang, X., Huang, F. All-Polymer Solar Cells with Efficiency Approaching 16% Enabled Using a Dithieno[3′,2′:3,4;2′′,3′′:5,6]benzo[1,2-c][1,2,5]thiadiazole (fDTBT)-Based Polymer Donor. J Mater Chem A. 2021;9:8975–8983.

10. Yang, F., Forrest, S. R. Photocurrent Generation in Nanostructured Organic Solar Cells. ACS Nano 2008;2:1022–1032.

11. Araújo, A. A. S., Bezerra, M. S., Storporitis, S., Matos, J. R. Determination of the melting temperature, heat of fusion, and purity analysis of different samples of zidovudine (AZT) using DSC. Braz J Pharm Sci 2010;1:46

12. Midori, K., Fukuhara, T., Tamai, Y., Kim, H. D., Ohkita, H. Enhanced Hole Transport in Ternary Blend Polymer Solar Cells. Chem Phys Chem 2019;20:2683–2688.

13. Hecht, K. Zum Mechanismus des Lichtelektrischen Primärstromes in Isolierenden Kristallen. Eur Phys J A. 1932;77:235–245.

14. Elizabeth, v. H., Vladimir, D., Jürgen, P. Study of Field Effect Mobility in PCBM Films and P3HT:PCBM Blends. Sol Energy Mater Sol Cells. 2005;87:149–156.

15. Yan, H., Chen, Z., Zheng, Y., Newman, C., Quinn, J. R., Dötz, F., Kastler, M., Facchetti, A. A High-Mobility Electron-Transporting Polymer for Printed Transistors. Nature 2009;457:679–686.

16. Nishi, T., Wang, T. T. Melting Point Depression and Kinetic Effects of Cooling on Crystallization in Poly(vinylidene fluoride)-Poly(methyl methacrylate) Mixtures. Macromolecules 1975;8909–915.

17. Flory, P. Principles of Polymer Chemistry. Cornell University Press: Ithaca, New York, 1971.

18. Kim, J. Y. Phase Diagrams of Ternary π-Conjugated Polymer Solutions for Organic Photovoltaics. Polymers 2021;13:983.

19. Flory, P. J. Thermodynamics of High Polymer Solutions. Chem Phys. 1942;10:51–61.

20. Huggins, M. L. Some Properties of Solution of Long-Chain Compounds. J Phys Chem. 1942;46:151–158.

21. Flory, P. J. Fifteenth Spiers Memorial Lecture. Thermodynamics of Polymer Solutions. Faraday Discuss. 1970;49:7–29.

22. Kim, J. H., Gadisa, A., Schaefer, C., Yao, H., Gautam, B. R., Balar, N., Ghasemi, M., Constantinou, I., So. F, O'Connor, B. T., Gundogdu, K., Hou, J., Ade, H. Strong polymer molecular weight-dependent material interactions: impact on the formation of the polymer/fullerene bulk heterojunction morphology. J Mater Chem A 2017;5:13176–13188.

23. Ghasemi, M., Hu, H., Peng, Z., Rech, J. J., Angunawela, I., Carpenter, J. H., Stuard, S. J., Wadsworth, A., McCulloch, I., You, W., Ade, H. Delineation of Thermodynamics and Kinetic Factors that Control Stability in Non-Fullerene Organics Solar Cells. Joule 2019;3:1328–1348.

24. Van Franeker, J. J., Hermida-Merino, D., Gommes, C., Arapov, K., Michles, J. J., Janssen, R. A. J., Portale, G. Sub-Micrometer Structure Formation during Spin Coating Revealed by Time-Resolved In Situ Laser and X-Ray Scattering. Adv Funct Mater 2017;27:1702516.

25. Biernat, M., Dąbczyński. P., Biernat, P., Rysz, J. Phase Separation in PCDTBT:PCBM Blends: from Flory-Huggins Interaction Parameters to Ternary Phase Diagrams. Chinese J Polym Sci 2020;38:1025–1033.

26. Van Franeker, J. J., Westhoff, D., Turbiez, M., Wienk, M. M., Schmidt, V., Janssen, R. A., J. Controlling the Dominant Length Scale of Liquid-Liquid Phase Separation in Spin-Coated Organic Semiconductor Films. Adv Funct Mater. 2015;25:855–863.

27. Wen, G., Zou, X., Hu, R., Peng, J., Chen, Z., He, X., Dong, G., Zhang, W. Ground- and Excited-State Characteristics in Photovoltaic Polymer N2200. RSC Adv. 2021;11:20191–20199.

28. Bartelt, J. A., Beiley, Z. M., Hoke, E. T., Mateker, W. R., Douglas, J. D., Collins, B. A., Tumbleston, J. R., Graham, K. R., Amassian, A., Ade, H., Fréchet, J. M. J., Toney, M. F., Mcgehee, M. D. The Importance of Fullerene Percolation in the Mixed Regions of Polymer-Fullerene Bulk Heterojunction Solar Cells. Adv Energy Mater. 2013;3:364–374.

29. Ye, L., Collins, B. A., Jiao, X., Zhao, J., Yan, H., Ade, H. Miscibility–Function Relations in Organic Solar Cells: Significance of Optimal Miscibility in Relation to Percolation. Adv Energy Mater. 2018;8:1703058.

30. Ye, L., Hu, H., Ghasemi, M., Wang, T., Collins, B. A., Kim, J.-H., Jiang, K., Carpenter, J. H., Li, H., Li, Z., Mcafee, T., Zhao, J., Chen, X., Lai, J. L. Y., Ma, T., Bredas, J.-L., Yan, H., Ade, H. Quantitative Relations between Interaction, Miscibility and Function in Organic Solar Cells. Nat Mater. 2018;17:253–260.

31. Lindvig, T., Michelsen, L, M., Kontogeorgis, M. G. A Flory-Huggins Model Based on the Hansen Solubility Parameters. Fluid Ph Equilibria. 2002;203:247–260.

32. Jalan, I., Lundin, L., Van Stam, J. Using Solubility Parameters to Model More Environmentally Friendly Solvent Blends for Organic Solar Cell Active Layers. Materials. 2019;12:3889.

33. Machui, F., Langner, S., Zhu, X., Abbott, S., Brabec, C, J. Determination of the $P3HT:PC_{61}BM$ Solubility Parameters via a Binary Solvent Gradient Method: Impact of Solubility on the Photovoltaic Performance. Sol Energy Mater Sol Cells. 2012;100:138–146.

Figure legends

Figure 1. (a) Chemical structures, (b) absorption spectra, and (c) energy diagrams of each material employed in this study.

Figure 2. J–V characteristics of P3HT-based (broken lines) and PDCBT-based (solid lines) solar cells with different acceptor materials.

Table 1. Photovoltaic parameters of P3HT-based and PDCBT-based solar cells.

Table 2. Photovoltaic parameters, PL quenching efficiencies, charge generation and collection efficiencies for the various polymer blends.

Figure 3. Normalized absorption spectra of (a-b) PCBM-based, (c-d) ITIC-based, and (e-f) N2200-based blends and each neat films. Gray and black solid lines represent donor and acceptor neat films, respectively. Each colored solid line represents donor/acceptor blend film, respectively.

Figure 4. J–V characteristics of (a) P3HT-based and (b) PDCBT-based polymer solar cells. Open circles and solid lines represent experimental data and the fitted curve, respectively.

Figure 5. DSC heat flow of PDCBT plotted against temperatures. Dotted and broken lines represent baseline and tangent at inflection point of the DSC curve, respectively. Red circle shows the intersection of the tangent and baseline, which gives the melting point T_m.

Table 3. χ parameters for the various blends of donor polymer, acceptor, and solvent at room temperature (300 K).

Figure 6. Ternary phase diagrams for three components of (a) solvent/P3HT/acceptor and (b) solvent/PDCBT/acceptor systems. Solid lines represent binodal line of each donor with PCBM (red), ITIC (green), and N2200 (blue). Broken lines correspond to a drying pathway at an acceptor fraction of 0.50 ($\varphi_{Donor} : \varphi_{Acceptor} = 1 : 1$). Open and closed circles represent the binodal point of each system and acceptor volume fraction in the mixed-phase, respectively.

Figure 7. Schematic illustration of phase-separated structure in mixed structure when $\varphi_{acceptor}$ is (a) low, (b) high, (c) $0.1 - 0.2$.

Figure 8. Illustration of the Flory–Huggins interaction parameter (χ)–volume fraction of acceptor (φ) phase diagram of (a) P3HT:PCBM and (b) P3HT:N2200 blends. Black solid line represents the binodal

line of each system.   The vertically highlighted area represents the percolation threshold of acceptor volume fraction.   The corresponding χ parameter is 1.4–1.9 for P3HT:PCBM and less than 0.01 for P3HT:N2200 blends, respectively.
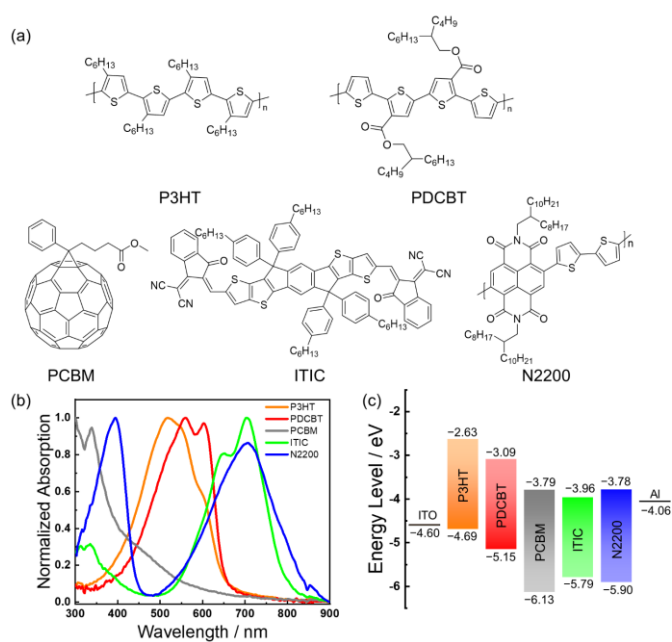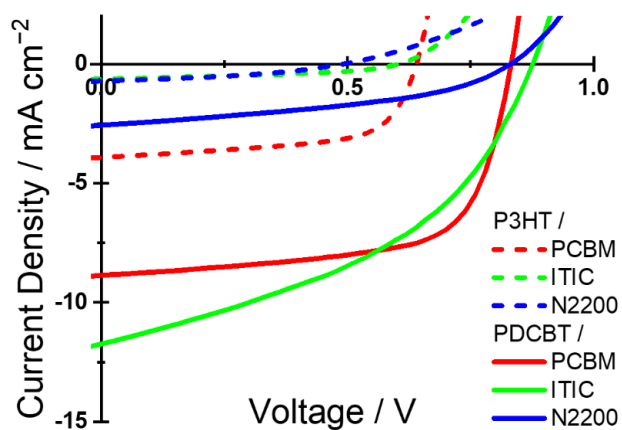
Display Items

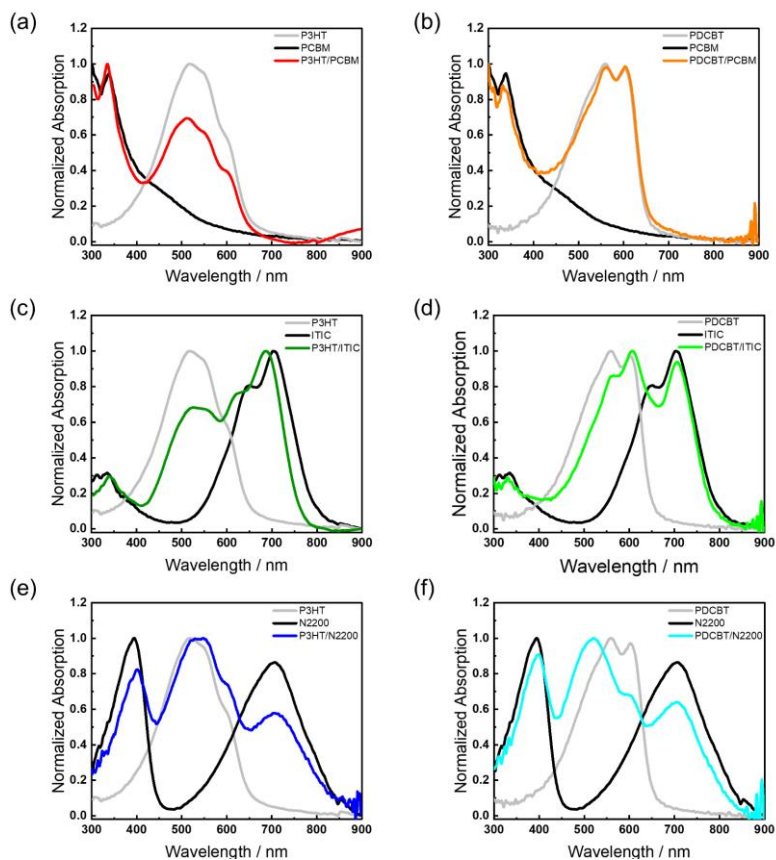**Figure 1.**

Figure 2.

Figure 3.

Figure 4.
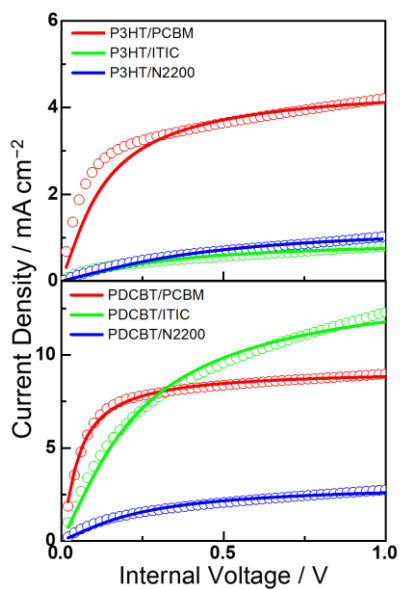
Figure 5.
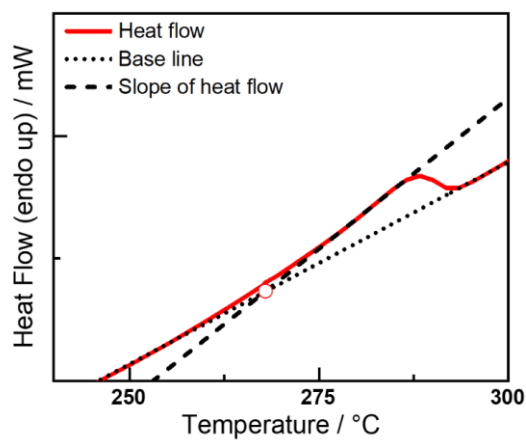
Figure 6.
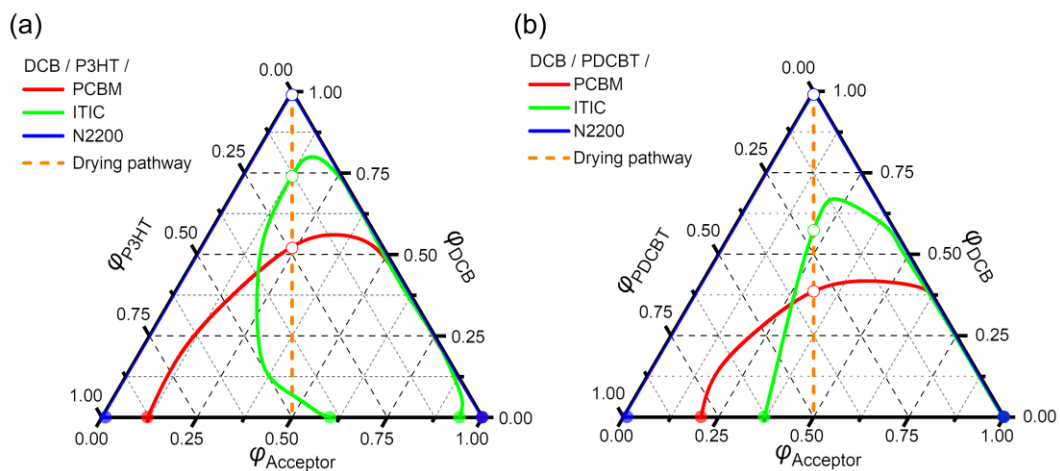
Figure 7.
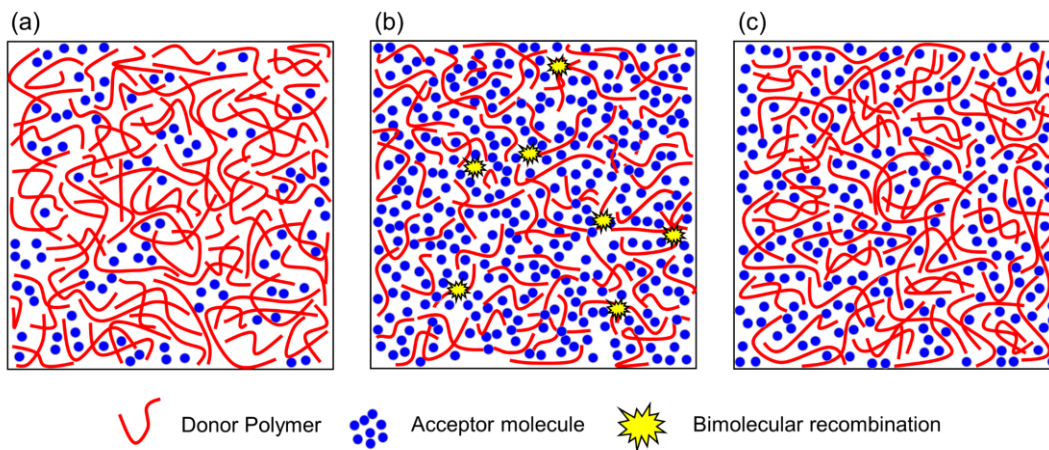
Figure 8.
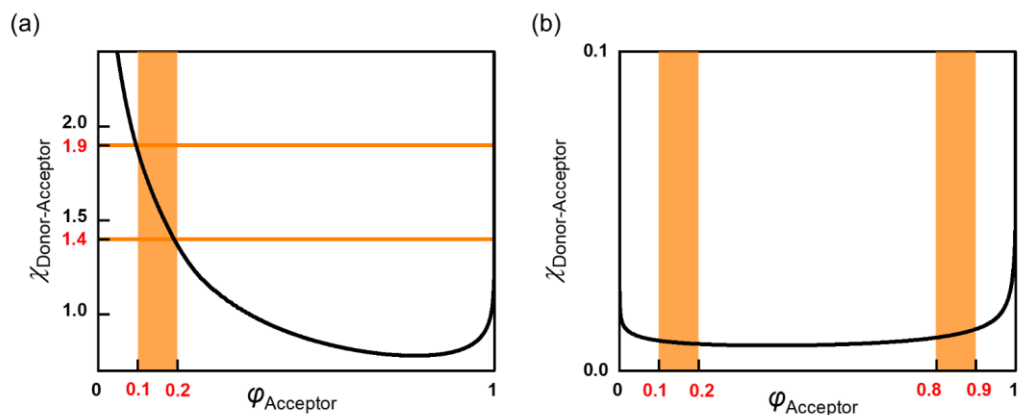
Table 1.

Donor	Acceptor	V_{OC} / V	J_{SC} / mA cm^{-2}	J_{SC}^{IPCE} / mA cm^{-2}	FF	PCE / %
P3HT	PCBM	0.64	3.9	4.7	0.63	1.6
	ITIC	0.60	0.63	0.99	0.43	0.16
	N2200	0.49	0.71	0.76	0.39	0.13
PDCBT	PCBM	0.83	8.9	8.72	0.66	4.9
	ITIC	0.88	11.7	11.96	0.43	4.4
	N2200	0.83	2.6	2.98	0.42	0.89

Table 2.

Donor	Acceptor	J_{SC} / mA cm^{-2}	FF	[1)]Φ_q^D / %	[2)]Φ_q^A / %	η_{CG} (η_{ED})	η_{CC}	η_{ED} η_{CC}
P3HT	PCBM	3.9	0.63	92	—	0.92	0.85	0.78
	ITIC	0.63	0.43	98	—	—	0.63	—
	N2200	0.71	0.39	47	3	0.014	0.51	0.0071
PDCBT	PCBM	8.9	0.66	96	—	0.96	0.97	0.93
	ITIC	11.7	0.43	96	67	0.64	0.79	0.51
	N2200	2.6	0.42	96	49	0.47	0.84	0.39

[1)] The samples were excited at 500 nm for selective excitation of donor polymers.
[2)] The samples were excited at 340, 700, and 700 nm for selective excitation of PCBM, ITIC, and N2200, respectively.

Table 3.

χ	P3HT	PDCBT	PCBM	ITIC	N2200
P3HT	—	—	1.68	0.84	0.17
PDCBT	—	—	1.34	1.01	0.17
DCB	0.17	0.34	0.67	0.84	1.68

Supplementary Information

Correlating Structure with Photovoltaic Properties in Phase-Separated Blends of Conjugated Donor Polymer and Acceptor

Jihun Jeon,[1] Kiyotaka Doi,[1] Hyung Do Kim,[1] Hiroki Ogawa,[2] Mikihito Takenaka,[2] Hideo Ohkita[1]

[1] Graduate School of Engineering, Department of Polymer Chemistry, Kyoto University, Katsura, Nishikyo-ku, Kyoto 615-8510, Japan.

[2] Institute for Chemical Research, Kyoto University, Gokasho, Uji, Kyoto 611-0011, Japan.

Contact

Hyung Do Kim: hyungdokim@photo.polym.kyoto-u.ac.jp

Hideo Ohkita: ohkita@photo.polym.kyoto-u.ac.jp

Figure S1. Photoelectron yield spectra of (a) P3HT, (b) PDCBT, (c) PCBM, (d) ITIC, and (e) N2200 films.
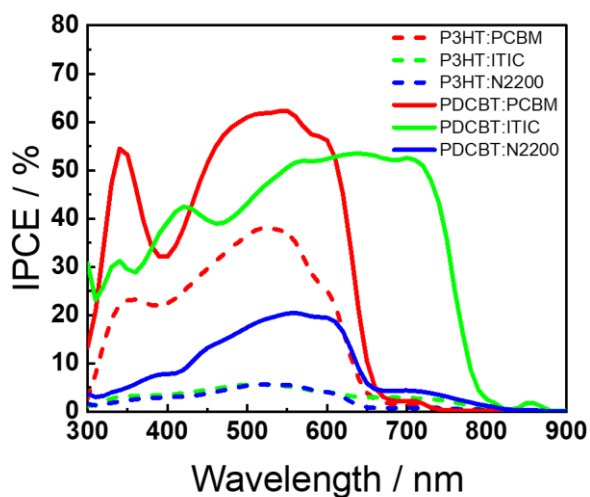

Figure S2. The IPCE spectra of polymer solar cells: P3HT/PCBM (red broken line), P3HT/ITIC (green broken line), P3HT/N2200 (blue broken line), PDCBT/PCBM (red solid line), PDCBT/ITIC (green solid line), and PDCBT/N2200 (blue solid line).
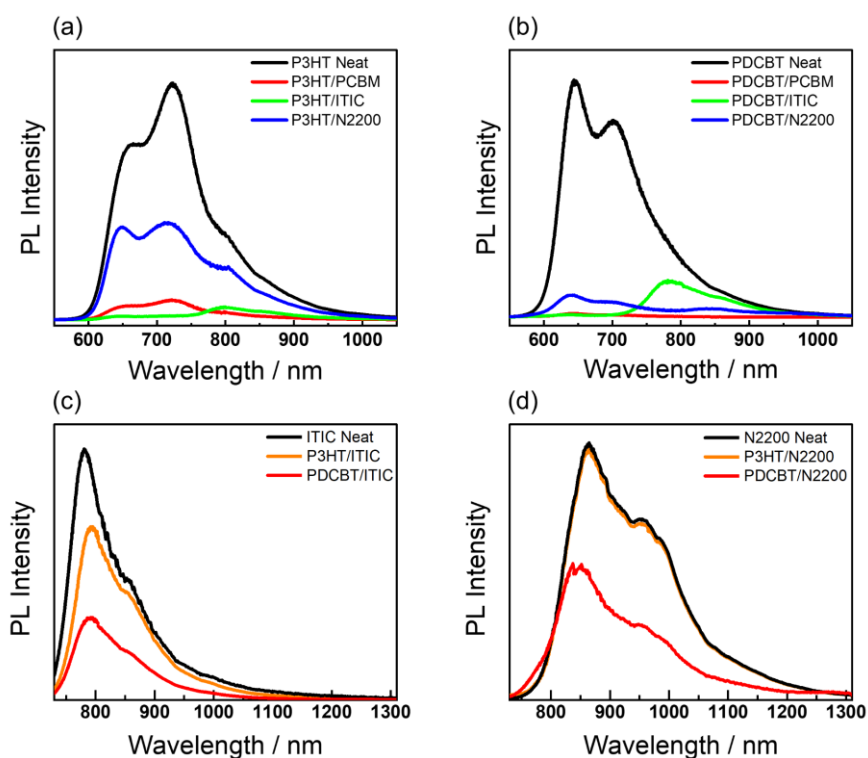
Figure S3. PL spectra of (a) P3HT in neat (black), in P3HT/PCBM (red), in P3HT/ITIC (green), and in P3HT/N2200 blends (blue), (b) PDCBT in neat (black), in PDCBT/PCBM (red), in PDCBT/ITIC (green), and in PDCBT/PCBM blends (red), (c) ITIC in neat (black), in P3HT/ITIC (orange), and in PDCBT/ITIC (red) blends, and (d) N2200 in neat (black), in P3HT/N2200 (orange), and in PDCBT/ITIC (red) blends.
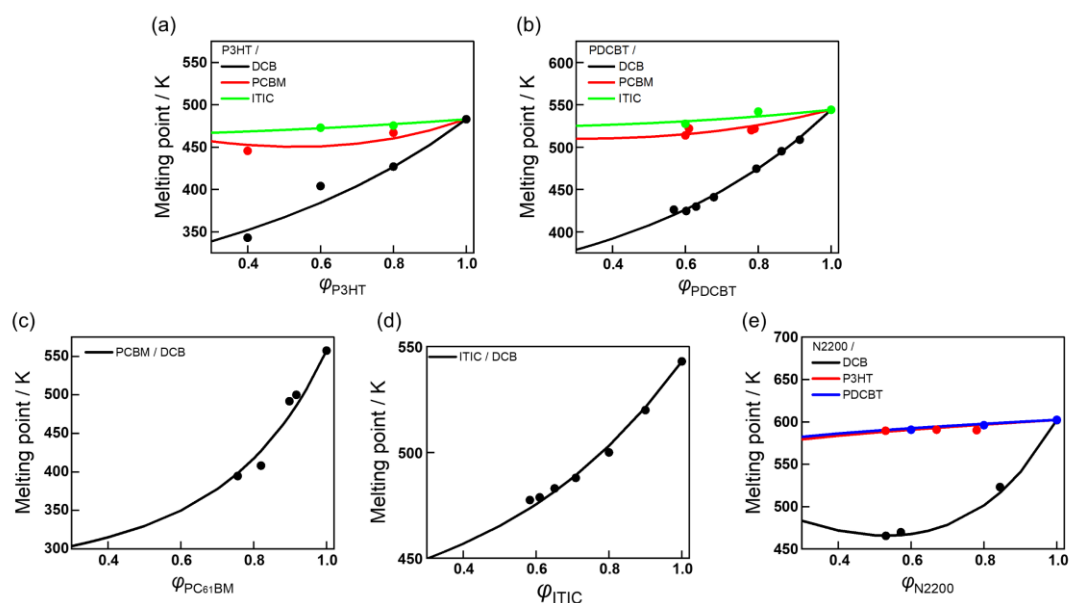

Figure S4. Melting point depression of (a) P3HT in DCB (black), in PCBM (red), and in ITIC (green), (b) PDCBT in DCB (black), in PCBM (red), and in ITIC (green), (c) PCBM in DCB, (d) ITIC in DCB, and (e) N2200 in DCB (black), in P3HT (red), and in PDCBT (blue).
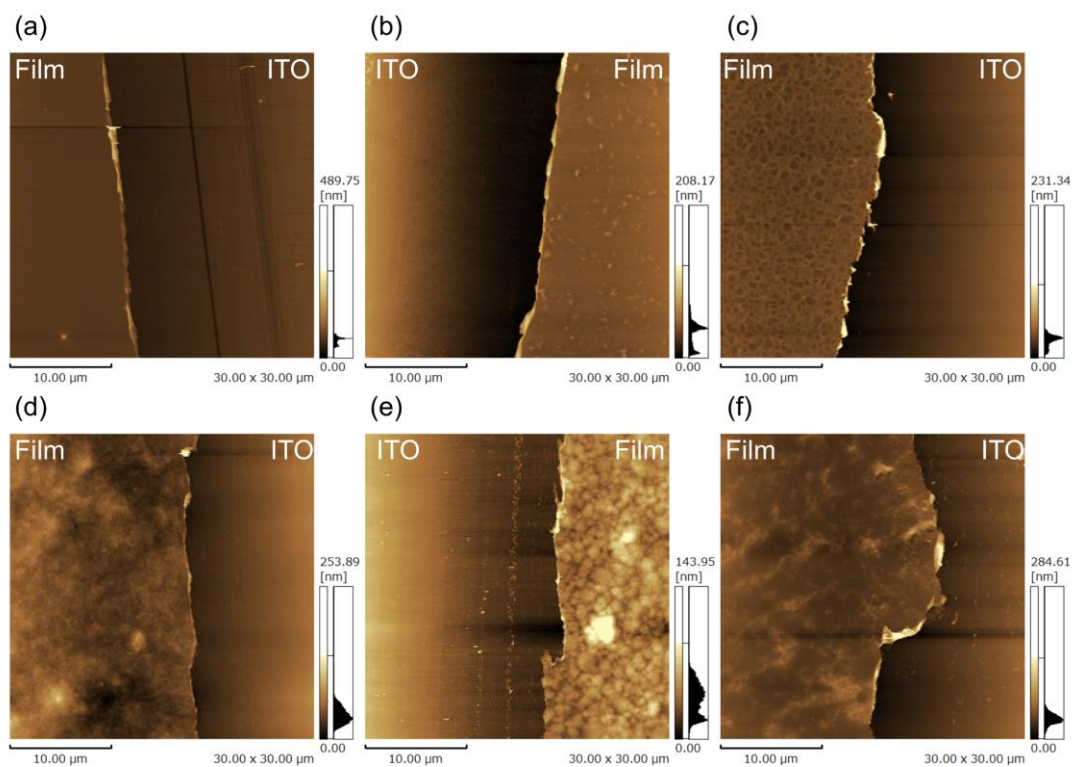
Figure S5. AFM images of (a) P3HT/PCBM, (b) P3HT/ITIC, (c) P3HT/N2200, (d) PDCBT/PCBM, (e) PDCBT/ITIC, and (f) PDCBT/N2200 blend films, respectively.
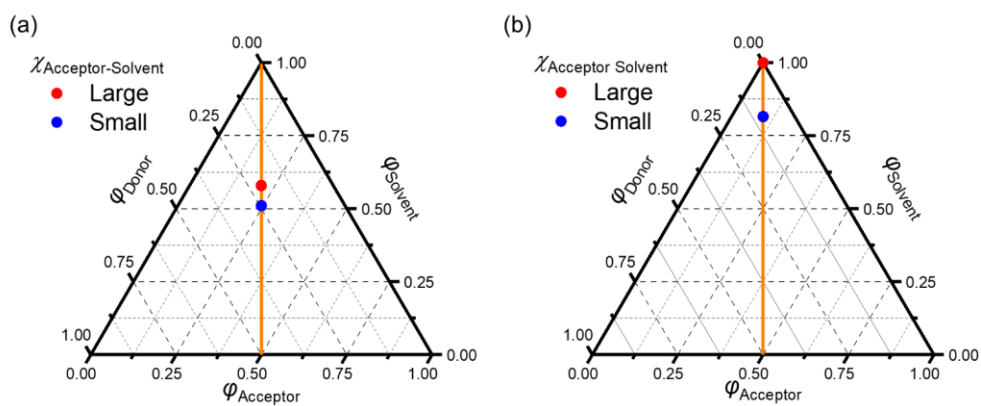

Figure S6. Ternary phase diagrams for three components of (a) solvent/P3HT/PCBM, (b) solvent/PDCBT/N2200 systems with different binodal points, respectively.
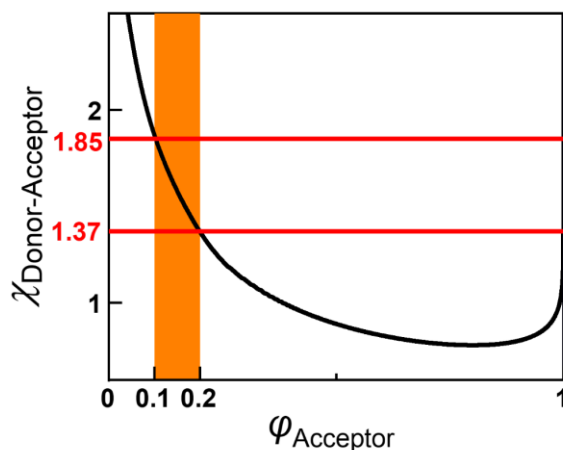
Figure S7. Illustration of the Flory–Huggins interaction parameter (χ)–volume fraction of acceptor (φ) phase diagram ofP3HT/ITIC blend according to the acceptor volume fraction. Black solid line represents the binodal line of correspond system. The vertically highlighted area represents the percolation threshold of acceptor volume fraction. The corresponding χ parameter is 1.37–1.85 for this system.

Table S1. Thermodynamic parameters used for the interaction parameter evaluation.

Material 1	Material 2	V_{1u}	V_{2u}	ΔH_{2f} / J g^{-1}	m_1	m_2
DCB		113			1	177
PCBM	P3HT	687	151	48	1	29
ITIC		929			1	22
DCB		113			1	193
PCBM	PDCBT	687	685	42	1	32
ITIC		929			1	23
	PCBM	113	687	15	1	6.1
DCB	ITIC	113	929	35	1	8.2
		113			1	434
P3HT	N2200	151	899	32	55	325
PDCBT		685			55	72

Table S2. The thickness of the polymer blend films.

Donor	Acceptor	Thickness
	PCBM	50
P3HT	ITIC	69
	N2200	59
	PCBM	53
PDCBT	ITIC	61
	N2200	50

Table S3. Solubility parameters of each component.

	δ_D / MPa$^{0.5}$	δ_P / MPa$^{0.5}$	δ_H / MPa$^{0.5}$	$\Delta\delta_{PCBM\text{-}Solvent}$	$\Delta\delta_{N2200\text{-}Solvent}$
PCBM	20.3	0.4	8.4	—	—
N2200	18.4	0.7	2.3	—	—
DCB	18.3	7.7	2.8	9.4	7.0
CB	18.0	4.3	2.0	7.8	3.6

Graphical Abstract